Supplementary Data

Estimating an LSPR Peak Shift with the Gouy-Chapman-Stern Model

An electrical double layer is created at the charged surface of an object upon immersion in a liquid. In a simplified model without distinction between the inner and outer Helmholtz planes (i.e. assuming specific adsorption), the layer of ions with opposite charge on the electrode surface is known as a Stern layer. This layer can be especially dense in the presence of an applied potential, which creates the initial potential drop. The remaining electric potential is then shielded by a second layer of ions known as the diffuse layer, since the weaker electrostatic interaction and thermal motion permits ion mobility. The electric potential attributed to the electrode decays approximately exponentially on a characteristic length scale, the Debye length κ^{-1}, which is inversely proportional to the square root of the ion concentration. Hence, the higher the ionic strength of a liquid, the more efficient the shielding of the electric potential, yielding a thinner double layer. This is illustrated in the figure below, Figure S1.

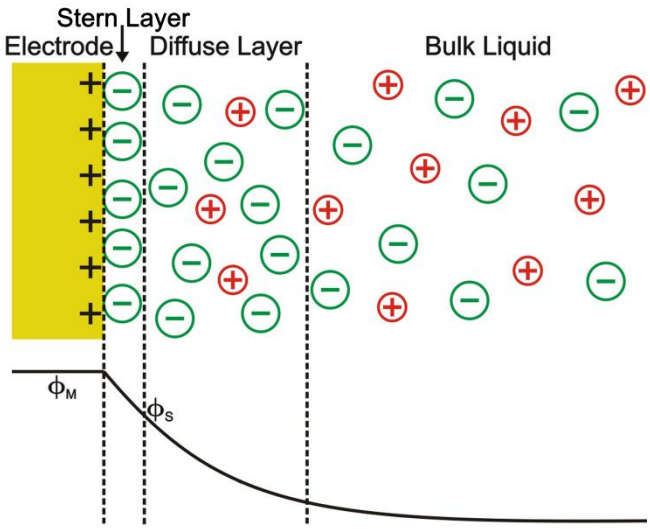

Figure S1. Schematic depiction of the double layer on an electrode immersed in a liquid. Coulomb interaction binds the ions in the Stern layer to the electrode surface. Ions in the diffuse layer are mobile, but compared to the bulk liquid the diffuse layer contains an excess of negatively charged ions. The distance-dependent potential of the double layer is indicated below. The parameter φ_M is the surface

potential of the electrode, whereas φ_S denotes the Stern potential. The value κ^{-1} represents the Debye length.

The combination of the Gouy-Chapman-Stern model with the Clausius-Mossotti (Lorenz-Lorentz) equation is shown in equation S1. It relates the refractive index of a substance to its polarizability, where n is the refractive index, N is the number of molecules per unit volume, and α is the mean polarizability.

$$\frac{n^2-1}{n^2+2} = \frac{4\pi}{3}\sum_i (N_i\alpha_i) \qquad 1$$

Equation S1. An adapted form of the Clausius-Mossotti (Lorenz-Lorentz) to calculate the refractive index at a given position as a function of the contributing ion polarizability and concentration values.

Consideration of the Gouy-Chapman-Stern model enables the formulation of ion concentration N as a function of distance from the electrode surface. In brief, this is achieved by first assuming a Stern layer potential, i.e. the potential at a distance from the surface equal to the size of the adsorbed ions. (This Stern layer potential is typically assumed to be around 100mV since higher potentials result in ion concentrations higher than that of a saturated solution.) The Gouy-Chapman theory then provides the potential decay with distance from the Stern layer. The ionic concentration as a function of distance from the surface is then calculated by the Boltzmann distribution. Once the concentration variations can be described, the corresponding refractive index changes are calculated using Equation 1. The Lorenz-Lorenz relation can also be applied to the Stern layer itself to estimate its effective refractive index. However, this requires that the number of adsorbed ions is known. This value can, in turn, be estimated from the potential drop over the Stern layer (surface potential minus Stern potential) by treating the layer as a capacitor where charges are separated by a distance equal to the radius of the ion.

Using this approach, the system is then analyzed in two states for 150 mM NaCl: At 0 mV the distribution of ions is assumed homogeneous and results in a constant value for the refractive index from the Clausius-Mossotti (Lorenz-Lorentz) equation. At 500 mV an electrical double layer is formed

and the distance-dependent ion concentration (i.e. at the Stern layer, as well in the diffuse layer) is represented in Equation S2 by the distance-dependent refractive index $n(z)$. The difference between these two states is then determined by integrating the product of the local refractive index and the local sensitivity over the distance from the surface.

$$\Delta\lambda_{Peak} = \int_0^\infty \Delta n(z) S(z) dz \qquad 2$$

Equation S2 – The change in the resonance wavelength is obtained by integrating the product of a system's sensitivity S and the change in refractive index Δn between two states (e.g. varied potentials, types of ions or ion concentrations) at all distances extending from the surface of an electrode.

In order to differentiate between the Stern layer and the diffuse layer, the Stern layer was assumed to have a thickness equal to the ionic diameter (0.362 nm) of chloride ions.[22] Here the Stern potential was assumed to be 80 mV when a potential of 500 mV was applied to the working electrode. With these potentials and low physiological salt concentrations (i.e. 150 mM NaCl) the maximum calculable refractive index value of 3.0 for the chloride Stern layer would be impossible to obtain, which assumes densely-packed chloride ions displacing all water molecules from the surface.[1] The bulk refractive index sensitivity and the field decay length of the system must also be known to estimate the sensitivity distribution s(z). The sensitivity distribution was assumed to decay exponentially. A simulation of the field decay length was performed by the multiple multipole program (MMP) using the MaX-1 software package and determined to lie between 4.2 nm and 6 nm.[2, 23] Since the diffusive layer at 150mM salt concentration (Debye length: 0.79 nm) is thinner than these values, a shorter field decay length results in a larger peak-shift.

So far the maximum measured bulk sensitivity for the nanowire arrays is 114.6 nm/RIU. Based on this value the maximum calculated peak shift due to the Stern and the diffusive layer was calculated to be 0.618 nm. Thus, it would be reasonable to conclude that a resonance shift of more than 2 nm, as shown in Figure 3, is very unlikely due only to a refractive index change in the surrounding medium.

This suggests that the attracted ions and Stern layer formation provoke an additional effect that contributes to the observed peak shifts in the combined optical and electrochemical measurements.

Nanofabrication

Extreme Ultraviolet Interference Lithography (EUV-IL) is a newly emerging nanolithography method that combines the advantages of a parallel fabrication process with high resolution. These features make it an attractive tool for researchers who are increasingly in need of nano-patterning capability that is beyond what is available from other methods such as photolithography, e-beam lithography (EBL), and scanning probe lithography, in terms of resolution or throughput. The used EUV-IL setup is part of the X-ray Interference Lithography (XIL) beamline of the Swiss Light Source (SLS). [3, 4]

The spatially coherent incident beam from an undulator is diffracted by a diffraction grating and the resulting fringe pattern produces lithographical patterning of resist on a wafer. The synchrotron light has a wavelength of 13.4 nm. The diffraction grating was fabricated by e-beam lithography and subsequent dry etching of a thin chromium film on top of a 100 nm thick silicon nitride support membrane, although EUV-IL itself can be used to create subsequent masks. Detailed information about the fabrication of the diffraction grating is provided by Auzelyte *et al.*.[5] The frequency of the resulting fringe pattern on the wafer is twice the frequency of the grating. Prior to exposure, 6 nm niobium oxide (Nb_2O_5) was thermally evaporated on glass wafers and spin coated a 40 nm thick PMMA film on top. This PMMA film was developed after the EUV-IL process in MIBK:IPA (1:3) solution. The nanowires of this work were created with the evaporation process as shown Figure S2.

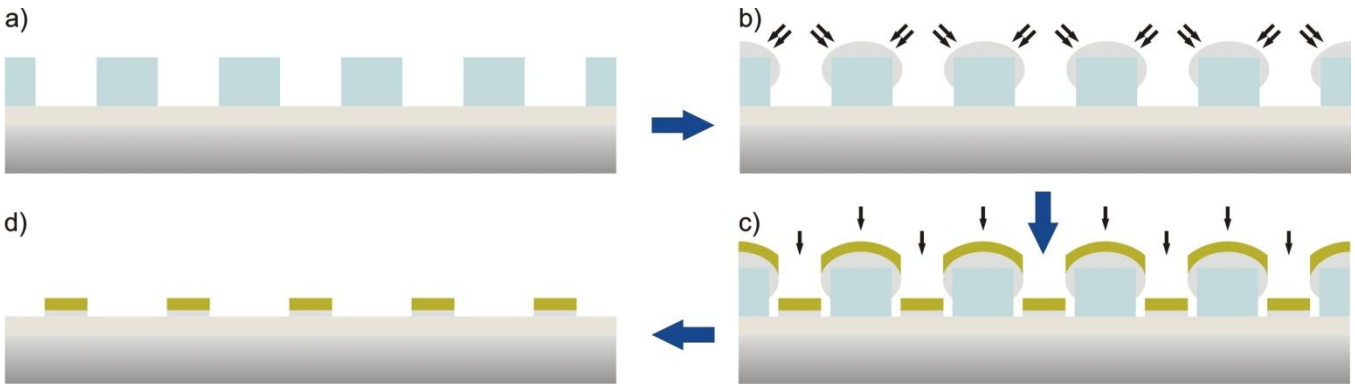

Figure S2 - a) PMMA line pattern fabricated by EUV-IL, b) Cr evaporated at an incident angle of 15°, c) Evaporation of Cr as intermediate layer and up to 50 nm of Au at normal incidence, d) Lift-off of the PMMA lines by NMP (N-Methylpyrrolidone) or acetone.

At the beginning, chromium was evaporated while the glass wafers were tilted by 15°. This forms a structure on top of the PMMA lines that prevents the subsequent deposited metal at normal incidence from covering the whole exposed substrate. Both chromium (2 nm) and gold (15 nm) were evaporated at a rate of 1 nm/s at a pressure of 2×10^{-6} mbar. The resulting line width of the gold wires is smaller than the gaps between the PMMA lines due to a shadowing effect. This under-cut profile is necessary for the final PMMA lift-off. The nanowire quality mainly depends on the resist pattern roughness, the properties of the metal and the conditions for metal deposition.

Microfabrication

In order to establish an electrical connection to the nanowire arrays, contact leads (e.g. width of 200 µm) were fabricated by conventional photolithography. The substrate was covered by a negative photoresist (ma-N 1400), spin-coated at 3000 RPM for 30 seconds and hardened by a soft-bake step for 2 minutes at 100°C. Mask alignment and exposure were performed in a Karl Süss X380 mask aligner for 120 seconds followed by a 1 hour long relaxing of the resist at room temperature. After removing the unexposed photoresist by immersion in ma-D 533/S developer for 120 seconds, 10 nm titanium and 40-50 nm gold were thermally evaporated. The photoresist was removed in 100% NMP. In a second photolithography step, the whole chip was again covered with S1805 photoresist and only one 50 µm ×

300 µm small window per nanowire array was opened. This step isolates the contact leads and most of the nanowire array, but opens a window to only a portion of the nanowire array between the contact pads for measurement. Example masks for the leads and contact pads, the windows and the resulting pattern within the nanowire region is shown in Figure S3.

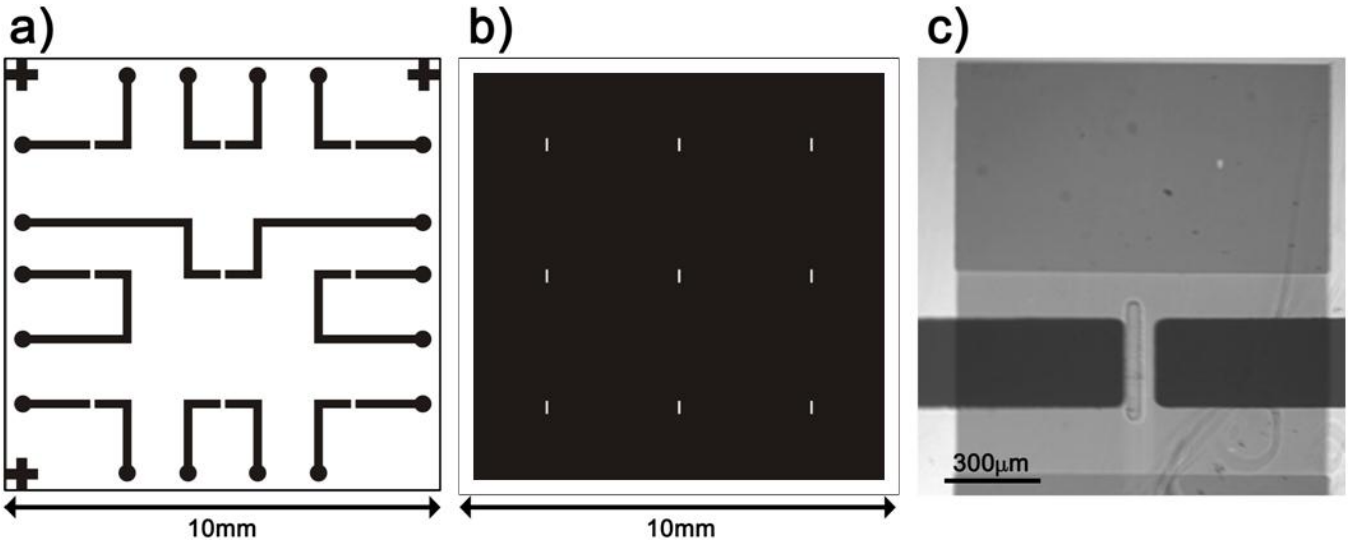

Figure S3 a) Contact lead mask. A negative photoresist was used and those regions unexposed to light were afterward removed in the developer solution. b) Window mask. For each nanowire array, one small window (e.g. 50 µm x 300 µm) was opened by this mask using a positive photoresist (e.g. S1805). This allows exposure of the nanowires to the fluid, while protecting and isolating the rest of the surface. c) Microscope image of a nanowire array. The window to the nanowires is placed between the two contact leads. The leads are separated by 100 µm, have a width of 200 µm and thus are potentially connected to 2000 individual nanowires (100 nm period).

Finally, specialized PCBs were fabricated to establish an electrical connection to the nanowire arrays, while still allowing optical interaction with the nanowire arrays. The contact leads were connected to the conductive paths of an inverted PCB by silver paste. Thus, the top-side of the chip and the windows to the nanowire arrays were completely separated from the electrical side of the PCB. Afterward the system was sealed by adding epoxy to the PCB/chip interface. The smooth back-side of the PCB was optimal for sealing with a PDMS flow cell. This interface is illustrated in Figure S4.

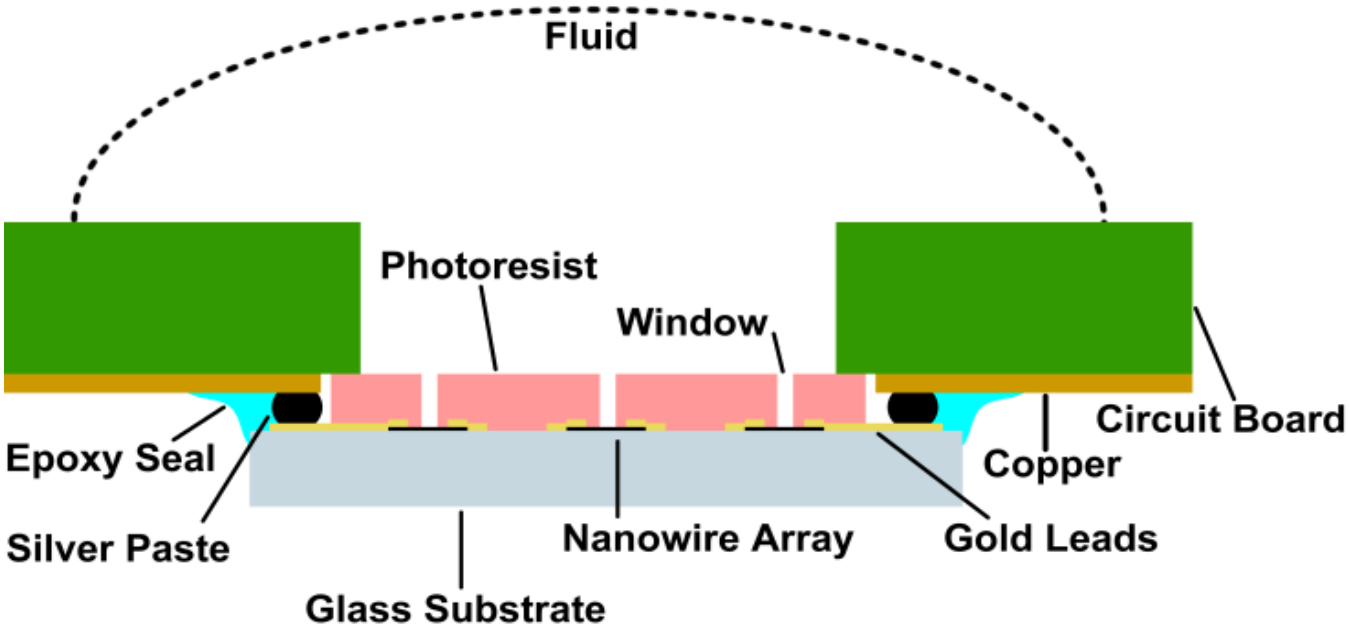

Figure S4 – The side-view schematic of the interface between the printed circuit board (PCB) and the optical nanowire chip. The liquids within the flow cell are isolated to the top and within the opening of the PCB. The nanowires are exposed to the liquid through an exposed opening (i.e. window) in the photoresist protective layer. The electrical interface is located on the underside of the PCB, which is completely separated from the liquid.

Flow cell

In order to expose the nanowire arrays to various fluids, a reusable flow cell was fabricated. A schematic of the assembled and disassembled flow cell is shown in Figure S5.

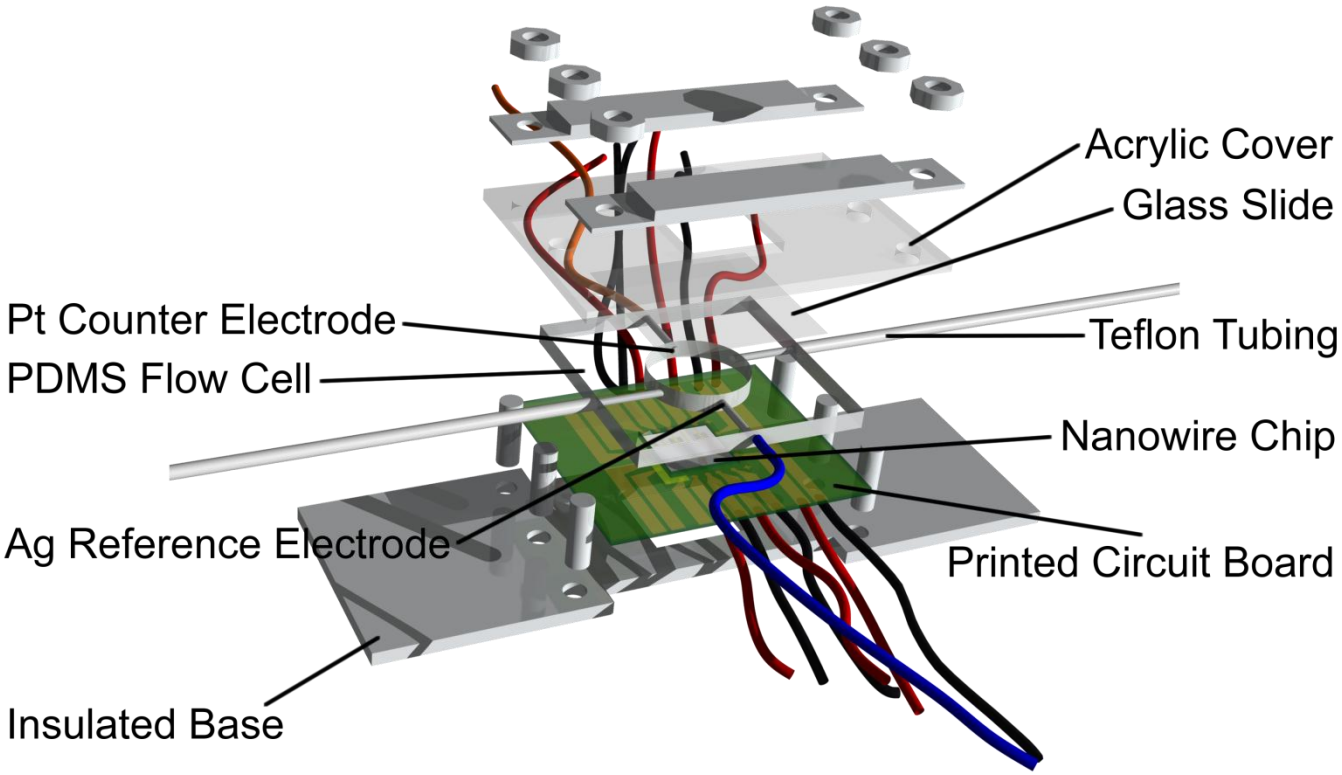

Figure S5 – A custom built electrochemical flow cell in its disassembled state. The flow cell itself consists of PDMS which is pressed against the PCB and sealed on the upper side by a glass slide. The flow chamber has a cylindrical shape (height: 2mm, diameter: 11mm) with a total volume of roughly 200µl. Two 0.8 mm Teflon tubes were inserted into two adjacent flow channels of the cell while a silver reference and a platinum counter reference electrode was placed into the remaining channels for electrochemical measurements.

Measurement system

Optical measurements were performed in an Axiovert 200 Microscope from Carl Zeiss, Germany. Light from a halogen lamp is guided through a condenser lens further through the nanowire array under investigation and focused by a 5x objective into a SpectraPro 2150 spectrometer (Princeton Instruments, US). The spectra were recorded by a PIXIS500 CCD camera (Princeton Instruments, US). All optical experiments were performed in this transmission geometry, as illustrated in Figure S6.

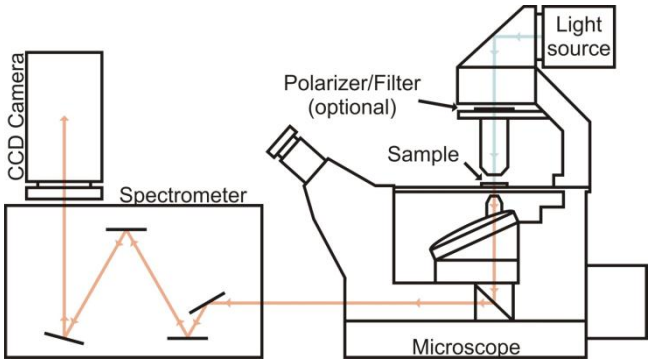

Figure S6 - optical measurement setup in transmission mode. Light is guided through a nanowire array into a spectrometer. Finally, the transmitted spectral intensity is recorded by a CCD camera.

Prior to each measurement, a background and a flat field image were recorded in order to remove artifacts from distortions in the optical path and variations in the sensitivity of the CCD camera. During the measurements, all fluids were manually pumped through the flow cell by syringes. The spectral intensity along a line within the opened photoresist window was recorded by WinSpec/32 software. Finally, the sequence of spectra was evaluated by custom-made software, which determined the position of the LSPR peak in each spectrum with different fitting functions.

For electrochemical measurements potentials were applied with a potentiostat (Model 2053, Amel Instruments, Italy). For the initial impedance spectroscopy experiments a second potentiostat (Autolab, Netherlands) was connected across the array. The impedance was measured over a frequency range of 0.1Hz-100 kHz with an applied AC amplitude of 10 mV (RMS). Both potentiostats have sufficiently high input impedances to avoid stray currents or system-dependent effects. Nonetheless, to experimentally eliminate any system dependencies or heating effects, a test circuit was constructed with a comparable resistor (28 Ω) to simulate the resistance of the nanowire array. The sodium chloride solution was modeled by a 100Ω resistor in series to a parallel connection of a 1 MΩ resistor and a 1 µF capacitor. The same 0, 500 mV and -500 mV potential cycle was applied twice to the 28Ω resistor, with no observable change related to the applied voltage, as is observable in Figure S7. Subsequent time-resolved measurements where measured with a lock-in amplifier (HF2LI, Zurich Instruments AG, Switzerland) at 80 Hz.

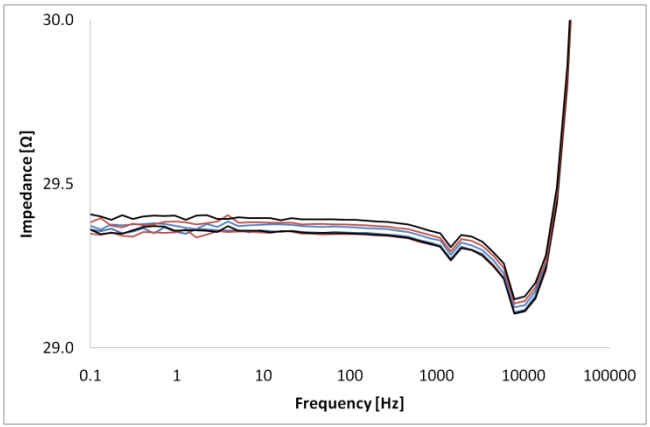

Figure S7 - Control measurements to eliminate system-dependent effects, such as heating or stray currents.

Electrochemical Equivalent Circuit of the Nanowire Array

Nevertheless, in order to rule out any perturbation from the potentiostats, the measurements were repeated in a control experiment, in which the nanowire array & sodium chloride solution were modeled by discrete elements. In detail, the nanowire array was replaced by a 28 Ω resistor and the sodium chloride solution was modeled by a test electrochemical circuit provided by Autolab (i.e. 1100 resistor in series to a parallel connection of a 1MΩ resistor and a 1μF capacitor). The same 0, -0.5, 0.5 V potential cycle was applied twice to the 28 Ω resistor modeling the nanowire array and no resistance change was observed. Additionally, an equivalent circuit (see Figure S8) was defined and matched to the measured data from the nanowire array. The elements R1, L1 and C1 model the impedance of the contact leads and the PCB lines whereas R2, L2 and C2 model one nanowire. The chosen width of the contact leads (200 μm contact width for nanowires with a 100 nm period) allows the connection of approximately 2000 nanowires in parallel. Initially the values of the equivalent circuit were fitted to the experimental data at an applied potential of 0 V. The fitting was performed with the NOVA1.5 software of the Autolab potentiostat. The magnitude and phase of the measured and simulated impedance can be seen in Figure S8. Then the values of R1, L1 and C1 were fixed and only the values attributed to the nanowires were fitted to the recorded data at a potentials of ±0.5V. Table S1 summarizes these values.

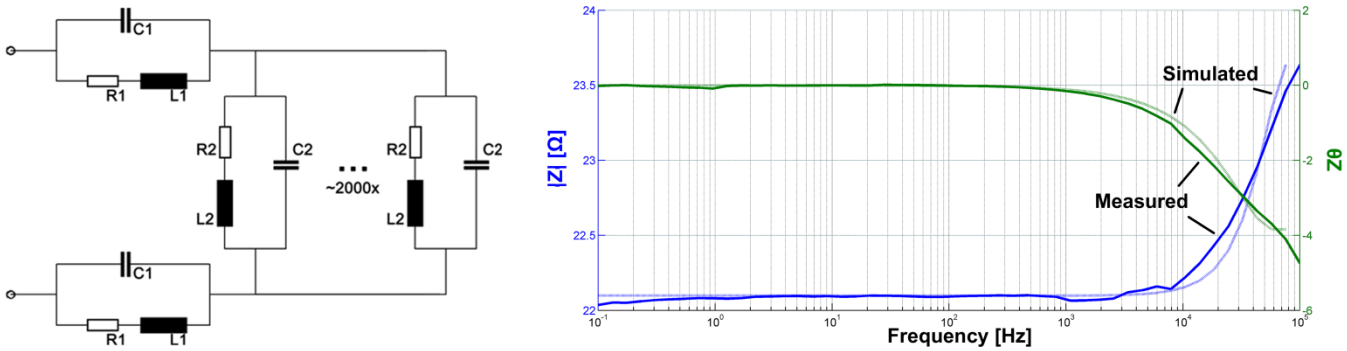

Figure S8 – a) The simulated equivalent circuit of the nanowire array (for 2000 parallel nanowires with a 100 nm period between contacts with a width of 200 μm) and contact impedance; b) The measured impedance of a nanowire array in 150 mM NaCl at 0V and the simulated impedance response of the equivalent circuit at 0V.

	-500 mV	**0 V**	**500 mV**
R1	2.8 Ω	2.8 Ω	2.8 Ω
L1	3.4 μH	3.4 μH	3.4 μH
C1	650 nF	650 nF	650 nF
R2	32.6 kΩ	32.8 kΩ	33.2 kΩ
L2	28.9 mH	28.9 mH	28.9 mH
C2	8.1 pF	8.0 pF	7.8 pF

Table S1 – The Extracted fitting parameters in order to match the equivalent circuit to the measured experimental data of a gold Au nanowire array in 150 mM NaCl at 0V.The elements . R1, L1 and C1 are of the measurement system and R2, L2 and C2 of the nanowire array. (see Figure S8)

References

1. Coker, H. *The Journal of Physical Chemistry* **2002,** 80, (19), 2084-2091.
2. Lide, D., *CRC Handbook of Chemistry and Physics, 88th Edition (Crc Handbook of Chemistry and Physics)*. CRC: 2007.
3. Solak, H. H. *Journal of Physics D-Applied Physics* **2006,** 39, (10), R171-R188.
4. Auzelyte, V.; Dais, C.; Farquet, P.; Grutzmacher, D.; Heyderman, L. J.; Luo, F.; Olliges, S.; Padeste, C.; Sahoo, P. K.; Thomson, T.; Turchanin, A.; David, C.; Solak, H. H. *Journal of Micro-Nanolithography Mems and Moems* **2009,** 8, (2), 10.
5. Auzelyte, V.; Solak, H. H.; Ekinci, Y.; MacKenzie, R.; Voros, J.; Olliges, S.; Spolenak, R. *Microelectronic Engineering* **2008,** 85, (5-6), 1131-1134.
6. Storhoff, J. J.; Elghanian, R.; Mucic, R. C.; Mirkin, C. A.; Letsinger, R. L. *Journal of the American Chemical Society* **1998,** 120, (9), 1959-1964.